# The genomic landscape, causes, and consequences of extensive phylogenomic discordance in Old World mice and rats

Gregg W. C. Thomas[1,2,*], Jonathan J. Hughes[3,4], Tomohiro Kumon[5], Jacob S. Berv[3,6], C. Erik Nordgren[5], Michael Lampson[5], Mia Levine[5], Jeremy B. Searle[3], Jeffrey M. Good[1]

[1]*Division of Biological Sciences, University of Montana, Missoula, MT, 59801.*

[2]*Informatics Group, Harvard University, Cambridge, MA, 02138*

[3]*Department of Ecology and Evolutionary Biology, Cornell University, Ithaca, NY, 14853.*

[4]*Department of Evolution, Ecology, and Organismal Biology, University of California Riverside, Riverside, CA, 92521*

[5]*Department of Biology, University of Pennsylvania, Philadelphia, PA, 19104*

[6] *Department of Ecology and Evolutionary Biology, University of Michigan, Ann Arbor, MI, 48109*

[*]Corresponding author

E-mail: gthomas@fas.harvard.edu

## Abstract

A species tree is a central concept in evolutionary biology whereby a single branching phylogeny reflects relationships among species. However, the phylogenies of different genomic regions often differ from the species tree. Although tree discordance is widespread in phylogenomic studies, we still lack a clear understanding of how variation in phylogenetic patterns is shaped by genome biology or the extent to which discordance may compromise comparative studies. We characterized patterns of phylogenomic discordance across the murine rodents (Old World mice and rats) – a large and ecologically diverse group that gave rise to the mouse and rat model systems. Combining recently published linked-read genome assemblies for seven murine species with other available rodent genomes, we first used ultra-conserved elements (UCEs) to infer a robust species tree. We then used whole genomes to examine finer-scale patterns of discordance and found that proximate chromosomal regions tended to have more similar phylogenetic histories. While we found no clear relationship between local tree similarity and recombination rates in house mice, we did observe a correlation between recombination rates and average similarity to the species tree. We also detected a strong influence of linked selection whereby purifying selection at UCEs led to less discordance. Finally, we show that assuming a single species tree can result in high error rates when testing for positive selection under different models. Collectively, our results highlight the complex relationship between phylogenetic inference and genome biology and underscore how failure to account for this complexity can mislead comparative genomic studies.

## Introduction

Phylogenies are the unifying concept in understanding the evolution of species, traits, and genes. However, with the availability of extensive high-throughput sequencing data it has become apparent that evolutionary relationships between species may not be well represented by a single representative phylogeny (Edwards 2009; Hahn and Nakhleh 2016). While a dominant signal of bifurcating speciation may exist (*i.e.*, a species tree), phylogenetic signal that may disagree with species relationships can arise from ancestral polymorphisms (incomplete lineage sorting; ILS), gene flow through hybridization (introgression), and gene duplication and loss (Maddison 1997). The theoretical prediction of phylogenetic discordance has long been appreciated (Hudson 1983; Pamilo and Nei 1988; Maddison 1997; Rosenberg 2002), but empirical evidence now emphasizes just how extensive discordance can be among a set of species. Several recent studies focused on analyzing phylogenetic discordance among the genomes of specific taxonomic groups (Feng et al. 2022; Gable et al. 2022; Smith et al. 2023). Among others, studies of birds (Jarvis et al. 2014), seals (Lopes et al. 2021), tomatoes (Pease et al. 2016), bumblebees (Sun et al. 2021), and butterflies (He et al. 2023) have found that with extensive taxon sampling and genomic data, highly supported species tree topologies are rarely or never recovered in the underlying locus trees. Whereas these examples highlight the prevalence of phylogenetic discordance across the tree of life, we still lack a clear understanding of how phylogenetic patterns are shaped by the details of genome biology or the extent to which discordance may compromise inferences from comparative studies that assume a singular species history.

From a practical perspective, failure to acknowledge and account for phylogenetic discordance could severely affect biological inference. Analyses of molecular evolution are usually performed on a gene-by-gene basis (Pond et al. 2005; Yang 2007; Hu et al. 2019; Kowalczyk et al. 2019), but it is still common practice to assume a single genome-wide species tree for each locus. For gene-based analyses, using the wrong tree may compromise inferences of positive directional selection, convergent evolution, and genome-wide inferences of correlated rate variation (Mendes et al. 2016). Phylogenetic discordance can also affect how continuous traits are reconstructed across phylogenies, as the genes that underly these traits may not follow the species history (Avise and Robinson 2008; Hahn and Nakhleh 2016; Mendes et al. 2018; Hibbins et al. 2023). In these instances, phylogenetic discordance may need to be characterized and incorporated into the experimental and analytical design. Alternatively, if a researcher's primary questions are focused on reconstructing the evolutionary history of speciation (*i.e.*, the species tree), then phylogenetic discordance may obscure the true signal of speciation (Fontaine et al. 2015). In this case, knowledge about patterns of discordance across genomes could inform decisions about locus selection, data filtering, and model parameters during species tree reconstruction.

Given these considerations, a better understanding of the genomic context of phylogenetic discordance is warranted. Although often conceptualized primarily as a stochastic consequence of population history (Maddison 1997), patterns of phylogenetic discordance are likely to be non-random and dependent on localized patterns of genetic drift, natural selection, recombination, and mutation. Discordance due to ILS ultimately depends on effective population sizes across the

branches of the phylogeny (Pamilo and Nei 1988; Degnan and Rosenberg 2006) and, therefore, should covary with any process that influences local patterns of genetic diversity (*e.g.*, linked negative or positive selection). Likewise, the potential for discordance due to introgression may be influenced by selection against incompatible alleles or positive selection for beneficial variants (Lewontin and Birch 1966; Jones et al. 2018). Selection, ILS, and introgression, are expected to leave differing signals across a sample of genomes that should allow us to test hypotheses about both the cause and the scale of phylogenetic discordance (Huson et al. 2005; Kulathinal et al. 2009; Green et al. 2010; Vanderpool et al. 2020). Yet the genomic context of phylogenetic discordance has remained elusive. For example, localized patterns of phylogenetic discordance should be influenced by patterns of recombination (Hudson and Kaplan 1988) and simulation studies posit that the closer two regions are in the genome, the more history they share (Slatkin and Pollack 2006; McKenzie and Eaton 2020). However, studies of mammals have been inconclusive regarding the relationship between phylogenetic discordance and recombination rates, ranging from no correlation in great apes (Hobolth et al. 2007) to a weak correlation in house mice (White et al. 2009). Some studies have also linked increased amounts of phylogenetic discordance to areas of the genome with lower recombination rates (Scally et al. 2012; Pease and Hahn 2013). More recently, Rivas-Gonzalez et al. (2023) have found a strong correlation between levels of ILS and recombination rate through a detailed study of the primate phylogeny. However, it remains unclear how phylogenetic discordance scales locally across the genome as a function of recombination and the strength of linked selection.

To investigate the causes and consequences of phylogenetic discordance, we took advantage of genomic resources available for house mouse (*Mus musculus*). This rodent species is one of the most important mammalian model systems for biological and biomedical research and is embedded within a massive radiation of Old World rats and mice (Murinae). This ecologically diverse and species-rich group is comprised of over 600 species and makes up >10% of all mammalian species, and yet is only about 15 million years old. Despite the power of evolution-guided functional and biomedical analysis (Christmas et al. 2023), few murine genomes have been sequenced outside of *Mus* and *Rattus*.

In the present work, we analyze recently sequenced genome sequences for seven murine rodent species (*Mastomys natalensis*, *Hylomyscus alleni*, *Praomys delectorum*, *Rhabdomys dilectus*, *Grammoyms dolichurus*, *Otomoys typus*, and *Rhynchomys soricoides*) sampled from across this radiation (Kumon et al. 2021). We combine these new genomes with previously sequenced rodent genomes and genomic resources from the *M. musculus* model system to study phylogenetic relationships within Murinae as well as the landscape of discordance along rodent chromosomes. We first inferred a species tree for these and other sequenced rodent genomes, focusing on signals derived from ultra-conserved elements (UCEs) to promote broader comparisons across genomes of variable quality. We then used whole genome sequences from a subset of these genomes, genetic maps, and annotation information from house mice to describe the genomic context of phylogenetic discordance across murine rodents and evaluate several hypotheses linking discordance to genetic drift, natural selection, and recombination. Finally, we

show how the use of a single species-tree impacts gene-level inferences from common molecular evolution tests for natural selection in these species.

## Methods

### *Sample collection and assembly*

We collected genomes from 16 murine species and 2 other rodents from several sources, including NCBI and several recently sequenced in Kumon et al. (2021) (see Table 1 for full list of samples and sources). We also report the sampling of *Otomys typus* (FMNH 230007) from Ethiopia in 2015. While DNA extraction and sequencing on the 10x Genomics platform for *O. typus* is the same as described in (Kumon et al. 2021), the library quality for this sample was too low for chromosome level assembly. Here, we instead assembled it into scaffolds with the express purpose of obtaining UCEs for phylogenetic analysis. Adapters and low-quality bases were trimmed from the reads using illumiprocessor (Faircloth 2013), which makes use of functions from trimmomatic (Bolger et al. 2014). All cleaned reads were de novo assembled using ABySS 2.3.1 (Jackman et al. 2017) with a Bloom filter (Bloom 1970) de Bruijn graph. The final *O. typus* scaffold assembly was 2.14GB (N50=9,211; L50=64,014; E-size=12,790).

In parallel, for six of these species (see Table 1; Fig. 1), we generated reference-based pseudo-assemblies with iterative mapping using an updated version pseudo-it v3.1.1 (Sarver et al. 2017) that incorporates insertion-deletion variation to minimize reference bias in our genome-wide phylogenetic analyses and to maintain collinearity between assemblies (https://github.com/goodest-goodlab/pseudo-it). We used the *Mus musculus* (mm10) genome as the reference for our pseudo-assembly approach. Briefly, pseudo-it maps reads from each sample to the reference genome with BWA (Li 2013), calls variants with GATK HaplotypeCaller (Poplin et al. 2018), and filters SNPs and indels and generates a consensus assembly with bcftools (Danecek et al. 2021). The process is repeated, each time using the previous iteration's consensus assembly as the new reference genome to which reads are mapped. In total, we did three iterations of mapping for each sample.

### *Ultraconserved element (UCE) retrieval and alignment*

To reconstruct a broad phylogeny of murine rodents, we combined our seven recently sequenced genomes with nine publicly available genomes from other Old World mice and rats (subfamily Murinae) as well as the genomes of two non-murine rodents, the great gerbil (*Rhombomys opimus*; (Nilsson et al. 2020) and the Siberian hamster (*Phodopus sungorus*; (Moore et al. 2022) as outgroups. We extracted UCEs from each species, plus 1000 flanking bases from each side of the element using the protocols for harvesting loci from genomes and the *M. musculus* UCE probe set provided with phyluce v1.7.1 (Faircloth et al. 2012; Faircloth 2016). In total, we recovered 2,632 unique UCE loci, though not all UCE loci were found in all taxa (Table 1).

We brought the extracted UCE sequences for each species into a consistent orientation using MAFFT v7 (Katoh and Standley 2013) and then aligned them using FSA (Bradley et al.

2009) with the default settings. We trimmed UCE alignments with TrimAl (Capella-Gutierrez et al. 2009) with a gap threshold of 0.5 and otherwise default parameters. We performed alignment quality checks using AMAS (Borowiec 2016). We processed all alignments in parallel with GNU Parallel (Tange 2018).

*Species tree reconstruction from UCEs*

We constructed a species-level rodent phylogeny with two approaches. First, using the alignments of all UCEs found in four or more taxa (2,632), we reconstructed a maximum-likelihood (ML) species tree with IQ-TREE v2.2.1 (Minh et al. 2020b). Each UCE alignment was concatenated and partitioned (Chernomor et al. 2016) such that optimal substitution models were inferred for individual UCE loci with ModelFinder (Kalyaanamoorthy et al. 2017). We also reconstructed individual gene trees for each UCE alignment. For all IQ-TREE runs (concatenated or individual loci), we assessed branch support with ultrafast bootstrap approximation (UFBoot) (Hoang et al. 2018) and the corrected approximate likelihood ratio test (SH-aLRT) (Guindon et al. 2010). We collapsed branches in each UCE tree exhibiting less than 10% approximated bootstrap support using the nw_ed function from Newick Utilities (Junier and Zdobnov 2010). We used these trees as input to the quartet summary method ASTRAL-III v5.7.8 (Zhang et al. 2018) to infer a species tree. We generated visualizations of phylogenies with R v4.1.1 (R Core Team 2021) using phytools v1.9-16 (Revell 2012) and the ggtree package v3.14 (Yu et al. 2017; Yu 2020) and its imported functions from ape v5.0 (Paradis and Schliep 2019) and treeio v1.16.2 (Wang et al. 2020).

We then used two methods to assess phylogenetic discordance across the reconstructed species tree. First, we calculated site and gene concordance factors (sCF and gCF) with IQ-TREE 2 (Minh et al. 2020a; Minh et al. 2020b) to assess levels of phylogenetic discordance between the inferred UCE trees and the concatenated species tree. gCF is calculated for each branch in the species tree as the proportion of UCE trees in which that branch also appears (Baum 2007). sCF represents the proportion of alignment sites concordant with a given species tree branch in a randomized subset of quartets of taxa (Minh et al. 2020a). We visualized gCF and sCF (Lanfear 2018) for each branch in each species tree using methods in R v4.3.0 (Lanfear 2018; R Core Team 2021). Next, we used PhyParts (Smith et al. 2015b) to identify topological conflict between the UCE trees and the species tree from ASTRAL-III. For this analysis, we rooted all trees with *Phodopus sungorus* as the outgroup using the nw_reroot function in the Newick Utilities (Junier and Zdobnov 2010) package and excluded 204 UCE trees that did not contain the outgroup.

*Divergence time estimation*

We used IQ-TREE 2's (Minh et al. 2020b) implementation of least square dating to estimate branch lengths of our species trees in units of absolute time (To et al. 2016). To improve divergence-time estimation, we used SortaDate (Smith et al. 2018) to identify a set of 100 UCE loci that exhibit highly clocklike behavior and minimized topological conflict with the concatenated species tree. We applied node age calibrations (Table 2) from Schenk et al. (2013)

and Steppan and Schenk (2017), which in turn were sourced from fossil calibrations described on Paleobiology Database (2011). As *Rattus* is paraphyletic, the maximum age is taken from the earliest crown group fossil on Paleobiology Database (2011). In contrast, the estimated *Rattus* node age from Schenk et al (2013) was used as the minimum age. Branch lengths were resampled 100 times to produce confidence intervals. To return a single solution, least square dating typically requires that one calibration be fixed and not a range. We selected one calibration node (here, the branch leading to Murinae) and estimated dates across the tree when this node is set to its minimum, its maximum, and its midpoint ages. On the midpoint calibrated tree, we plot confidence intervals for each node representing the lowest minimum and highest maximum ages estimated across the three dating analyses.

*Genome window-based phylogenetic analysis*

To assess the distribution of phylogenetic discordance across the rodent genome, we limited subsequent analyses to *M. musculus* and the pseudo-assemblies (see above) of six of the genomes (*Mastomys natalensis*, *Hylomyscus alleni*, *Praomys delectorum*, *Rhabdomys dilectus*, *Grammomys dolichurus*, and *Rhynchomys soricoides*). *Otomys typus* was excluded from these analyses due to the inadequacy of the library outlined above.

We partitioned these genomes into 10 kilobase (kb) windows based on the coordinates in the reference *M. musculus* genome (mm10; Mouse Genome Sequencing et al. 2002) using bedtools makewindows (Quinlan and Hall 2010). These coordinates were converted between the reference and the consensus sequence for each genome using liftOver (Hinrichs et al. 2006). Note that this method assumes both collinearity of all genomes and similar karyotypes (see Discussion). We then removed windows from the subsequent analyses if (1) 50% or more of the window overlapped with repeat regions from the *M. musculus* reference RepeatMasker (Smit et al. 2013-2015) file downloaded from the UCSC Genome Browser's table browser (Hinrichs et al. 2006) or (2) 50% or more of the window contained missing data in 3 or more samples. Overlaps with repeat regions were determined with bedtools coverage (Quinlan and Hall 2010). We then aligned the 10kb windows with MAFFT (Katoh and Standley 2013), trimmed alignments with trimAl (Capella-Gutierrez et al. 2009), and inferred phylogenies for each with IQ-TREE 2 (Minh et al. 2020b) which uses ModelFinder to determine the best substitution model for each window (Kalyaanamoorthy et al. 2017).

To assess patterns of tree similarity between windows on the same chromosome, we used the weighted Robinson-Foulds (wRF) (Robinson and Foulds 1981; Böcker et al. 2013) distance measure implemented in the phangorn library (Schliep 2011) in R (R Core Team 2021), which compares two trees by finding clades or splits present in one tree but not the other weighted by the missing branch length in each tree for each mismatch and differences in branch length between the co-occurring branches in both trees (Robinson and Foulds 1979). Consequently, the resulting measure of wRF is in units of branch length (i.e., expected number of substitutions per site for maximum likelihood trees). We compared wRF between trees from windows on the same chromosome to characterize (1) heterogeneity in patterns discordance along the chromosome and

(2) whether tree similarity is correlated with distance between windows. For the second question, we sampled every window on a chromosome at increasing distance (in 10kb windows) until the distribution of wRF scores for all pairs of windows at that distance was not significantly different (Wilcox test, $p > 0.01$) than that of a sample of 12,000 measures of wRF between randomly selected trees on different chromosomes. We selected 12,000 as the random sample size because it roughly matched the number of windows on the largest chromosome (chromosome 1, n = 12,113). We used Snakemake 7 (Mölder et al. 2021) to compute window alignments and trees in parallel.

*Whole genome alignment between mouse and rat*

We used minimap2 (Li 2018) to align the mouse (mm10) and rat (rnor6) (Gibbs et al. 2004) genomes to assess the impact of structural variation that spans the divergence of our subset of species used to in the discordance analyses. We downloaded the rat reference genome (rnor6) from the UCSC genome browser and for both genomes removed the Y chromosome and all smaller unplaced scaffolds. We then used minimap2 in whole genome alignment mode (-x asm20) to generate a pairwise alignment file from which we calculated alignment segment sizes and the distances between alignment segments. We visualized the alignment as a dot plot using the pafr package in R (https://github.com/dwinter/pafr).

*Recombination rate and functional annotation*

We retrieved 10,205 genetic markers generated from a large heterogenous stock of outbred mice (Shifman et al. 2006; Cox et al. 2009) to assess whether phylogenetic discordance along chromosomes was correlated with mouse recombination rates. We converted the physical coordinates of these markers from build 37 (mm9) to build 38 (mm10) of the *M. musculus* genome using liftOver (Hinrichs et al. 2006). We then partitioned the markers into 5Mb windows and estimated local recombination rates defined as the slope of the correlation between the location on the *M. musculus* genetic and physical maps for all markers in the window (White et al. 2009; Kartje et al. 2020). Within each 5Mb window, we calculated wRF distances between the first 10kb window and every other 10kb window.

We also compared the chromosome-wide wRF distances to those based on phylogenies from regions around several types of adjacent to genomic features. We retrieved coordinates from 25,753 protein coding genes annotated in *M. musculus* from Ensembl (release 99; Cunningham et al. 2022), all 3,129 UCEs from the *M. musculus* UCE probe set provided with PHYLUCE (Faircloth et al. 2012; Faircloth 2016), and 9,865 recombination hotspots from Smagulova et al. (2011). The recombination hotspot coordinates were converted between build 37 and build 38 using the liftOver tool (Hinrichs et al. 2006). For each feature, the starting window was the 10kb window containing the feature's midpoint coordinate. We then calculated wRF between this window and all windows within 5Mb in either direction and for each chromosome compared the slope and wRF distance of windows adjacent to the feature with the same metrics for the whole

chromosome. We compared distributions of these measures for each genomic feature with an ANOVA (aov(feature.measure ~ feature.label)) followed by Tukey's range test (TukeyHSD(anova.result)) to assess differences in means, as implemented in R v4.1.1 (R Core Team 2021).

*Molecular evolution*

To test how tree misspecification affects common model-based analyses of molecular evolution, we retrieved 22,261 coding sequences from *M. musculus* using the longest coding transcript of each gene. Coding coordinates from the *M. musculus* coding sequences were transposed to the new assemblies via liftOver (Hinrichs et al. 2006) and sequences retrieved with bedtools getfasta (Quinlan and Hall 2010). We recovered 17,216 genes that were present in all 7 species. Using MACSE (Ranwez et al. 2018), we trimmed non-homologous regions from each ortholog using trimNonHomologousFragments, aligned the orthologs using alignSequences, and trimmed the aligned sequences with trimAlignment to remove unaligned flanking regions. Finally, we manually filtered the alignments using the following (non-mutually exclusive) criteria: 3,368 alignments were removed during filtering for gapped sites, 3,132 alignments had a premature stop codon in at least one species, 1,571 alignments had only 3 or fewer unique sequences among the 7 species, and 78 alignments were shorter than 100 bp. After filtering, 12,559 total alignments for tree reconstruction and inference of selection.

We then used IQ-TREE 2 (Minh et al. 2020b) to reconstruct a single species tree from concatenation of all gene alignments, as well as gene-trees for each individual alignment. This species tree from coding regions matches the topologies of these species inferred by concatenation of UCEs in the previous section. Next we ran several tests that use both coding alignments and a tree to infer positive selection: PAML's M1a vs. M2a test (Yang 2007), HyPhy's aBSREL model (Smith et al. 2015a), and HyPhy's BUSTED model (Murrell et al. 2015). We ran each test twice on each gene, once using the species tree derived from concatenated data, and once using the tree estimated for that gene. For the HyPhy models, no target branch was selected, meaning all branches in the input phylogeny were tested.

The end point of each of each of these three tests is a p-value, which lets us assess whether a model that allows for positively selected sites fits better than a model that does not. For M1a vs. M2a, we obtained the p-value manually by first performing a likelihood ratio test to determine genes under selection by calculating $2 * (lnl\ M1a - lnl\ M2a)$. The p-value of this likelihood ratio is then retrieved from a one-tailed chi-square distribution with 2 degrees of freedom (Yang 2007). For BUSTED and aBSREL, p-values are computed automatically during the test using similar likelihood ratios. For the M1a vs. M2a and BUSTED tests, a single p-value is computed for each gene. P-values were adjusted by correcting for false discovery rates (Benjamini and Hochberg 1995; Yekutieli and Benjamini 1999) using the "fdr" method in the p.adjust() function in R (R Core Team 2021) and we categorized a gene as being positively selected if its adjusted p-value was < 0.01. For the aBSREL test, a p-value is generated for each branch in the input gene tree. aBSREL corrects for multiple testing internally across branches using the Holm-Bonferroni

procedure (Holm 1979; Pond et al. 2005). We further correct the p-values across genes with the Bonferroni method and classify a gene as having experienced positive selection if one or more branches has a p-value < 0.01 after all corrections. We used Snakemake 7 (Mölder et al. 2021) to compute coding alignments, trees, and selection tests in parallel.

## Results

### *Murine species tree*

Using a concatenated dataset of 2,632 aligned ultra conserved elements (UCEs), we inferred a species tree (Fig. 1) that recovered the same relationships as previous reconstructions of Murinae using a small number of loci (Lecompte et al. 2008; Steppan and Schenk 2017). The species tree inferred from a quartet-based summary of the gene tree topologies was identical to the concatenated tree (Fig. S1).

While bootstrap and SH-aLRT values provided high support to our inferred species trees (Fig. 1), we found evidence for discordance across individual UCE phylogenies. The five shortest branches in the concatenated tree had a site concordance factor (sCF) of less than 50%, suggesting that alternate resolutions of the quartet had equivocal support (Fig. S2). Gene concordance factors (gCF) for each branch in the species tree were on aggregate much higher, with all but four branches supported by almost every gene tree in the analysis and with the lowest values likely being driven by a several short internal branches (Fig. S2). This pattern was recapitulated using a quartet-based summary method (Figs. S1 and S3). At the two most discordant nodes (E and J in Fig. 1), the recovered topology was supported by approximately one third of all gene trees.

We estimated divergence times for the inferred concatenated phylogeny (Fig. 1; Table S1) using four fossil calibration points (Table 2). The murid and cricetid groups had an estimated divergence time of 22.62 Ma (node A in Fig. 1) followed by the Murinae and the Gerbillinae at 21.30 Ma (B), albeit with wide confidence intervals in both cases. With the ancestral Murinae node (C) fixed for calibration, Hydromyini arose at 12.12 Ma (D) and was followed by Otomyini and Arvicanthini at 11.67 Ma (E). The remaining Murine tribes evolved in rapid succession, with Apodemini diverging at 10.82 Ma (F) and Murini and Praomyini splitting at 10.08 Ma (H). The *Rattus* node, which was fossil calibrated, was recovered at the very youngest end of the calibration range.

### *The landscape of phylogenetic discordance along murine genomes*

Next, we described the genomic landscape of phylogenetic discordance in murines and its relationship to local genomic features. To do this, we analyzed genome-wide phylogenetic histories of six recently sequenced murine rodent genomes and the *M. musculus* reference genome (see Fig. 1). Using the *M. musculus* coordinate system, we partitioned and aligned 263,389 non-overlapping 10 kb windows from these seven species (Table 1). After filtering windows in repetitive regions or with low phylogenetic signal, we recovered 163,765 trees with an average of 616 informative sites per window (Fig. S4).

Phylogenetic discordance was pervasive within and between chromosomes. We inferred 597 of the 945 possible unique rooted topologies among 6 species (when specifying *R. soricoides* as the outgroup) across all chromosomes (Table 3 shows the most common topologies recovered). The number of unique topologies per chromosome ranged from 75 to 218 with an average of 141 (Table 4), however, just four different topologies were ranked in the top three per chromosome. (Fig 2A; Table 3; File S1) and only nine trees were present at a frequency above 1%. Among these, the top three topologies only differed in the ordering of the clade containing *Hylomyscus alleni, Mastomys natalensis,* and *Praomys delectorum* (HMP clade) with the rest of the tree being consistent with the species tree. This clade also showed the second lowest concordance in the species tree inferred from UCEs (Fig. 1, node J). These three topologies comprise between 13-15% of all recovered topologies (Fig. 2). Interestingly, the least common of these three trees (13.1%) matched the topology recovered via concatenation of all coding regions and the species tree recovered from UCEs (Fig. 1). That is, the robustly inferred species tree did not match the evolutionary relationships inferred for over 85% of the genome.

While visual inspection revealed no clear partitioning of topological structures along chromosomes (*e.g.*, Fig. 2C), we found that phylogenies were not randomly distributed across mouse chromosomes. Using the weighted Robinson-Foulds metric, we found that tree similarity between windows decayed logarithmically along chromosomes (Fig. 3A and B) and the distance at which tree similarity appeared random varied considerably among chromosomes ranging from 0.15 Megabases (Mb) on chromosome 17 to 141.29 Mb on the chromosome 2 (Fig. 3C, Fig. S5). While chromosomes 2, 7, 9, and 11 were autosomal outliers with distances between windows to random-like trees exceeding 25 Mb, the average distance among all other autosomes was only 2.1 Mb. The rates at which phylogenetic similarity decayed tended to be inversely proportional to the distance at which two randomly drawn phylogenies lost similarity (Fig. 3D).

Next we aligned the reference genomes of mouse and rat to assess how large structural variation, such as inversions and translocations, may influence our inferences of phylogenetic relatedness along the genome. These species span the divergence of the sample for which we assessed genome-wide discordance, so the level of large structural variation present among them should give us an idea of the amount of ancestral variation in our sample. The mouse and rat genomes were mostly co-linear for large, aligned chunks, with large translocations and inversions on mouse chromosomes 5, 8, 10, 13, and 16 (Fig. S6). We also observe large-scale inversions on chromosome 16. We found that, while co-linearity of most chromosomes is conserved between mouse and rat, the size of the 300,000 aligned chunks averages under 10 kb, with the average distance between aligned segments being between 2,380 bp on the mouse genome and 4927 bp on the rat chromosome (Fig. S7). This pattern presents two major implications for our analyses. First, we could not transpose the coordinate system from mouse to rat with enough resolution to use genetic maps from rat. Second, most other structural variation in our sample appears likely to be small insertions of transposable elements (SINES which are about 150-500 bp in length and LINES which are about 4-7kb in length (Platt et al. 2018) that should have a negligible effect on our

discordance analyses since our window size is much larger and we excluded windows that were made up of mostly repeats.

*Discordance with recombination rate and other genomic features*

Using markers from genetic crosses within *M. musculus* (Shifman et al. 2006; Cox et al. 2009) we examined whether regions of the genome with high recombination also showed more phylogenetic discordance over short genetic distances when compared to regions with low recombination. Specifically, we calculated recombination rates within 5 Mb windows (Fig. S8) and then measured tree similarity between the first and last 10 kb window ($R^2$ = 3.0e-9; $p$ = 0.99; Fig. 4A) and the rate at which tree similarity changes between the first 10kb window and every other 10kb window ($R^2$ = 0.003; $p$ = 0.11; Fig. 4B). Surprisingly, we found no relationship between tree similarity and recombination rates measured at this scale. However, we did observe a slight positive correlation between recombination rate and similarity to the species tree when averaging wRF over all 10kb window trees within a 5Mb recombination window ($R^2$ = 0.05; $p$ = 7.6e-8; Fig. 4C). We also examine regions of the genome centered on so-called recombination hotspots identified in *M. musculus* and found that they had significantly slower rates of decay in similarity over genomic distance compared to windows that were not centered on hotspots ($p$ = 0.019; Fig. 5A), and that they were also significantly more phylogenetically similar over short distances ($p$ = 0.015; Fig. 5B). Thus, when taken as a whole, we found that windows with higher recombination rates in house mice did not show more local phylogenetic discordance but did show a general trend towards more phylogenetic discordance relative to the genome-wide species tree.

Evolutionary relationships around certain conserved genomic features may also be shaped by locally reduced effective population sizes due to a history of pervasive linked negative or positive selection. To test for this, we measured tree similarity in 10 kb windows around all annotated protein-coding genes, ultra-conserved elements (UCEs), and protein-coding genes identified as evolving rapidly (*i.e.*, significantly elevated $d_N/d_S$) due to positive directional selection and compared these patterns relative to chromosome-wide trends. We found that phylogenetic similarity around protein-coding genes was similar to that of windows without any genomic features (Fig. 5B), but that this similarity decayed more rapidly around genes ($p$ = 6.38e-8; Fig. 5A). Notably, UCEs showed the opposite pattern with much more similarity among adjacent windows than regions surrounding recombination hotspots ($p$ = 2.42e-12), coding genes ($p$ = 4.65e-14), rapidly evolving coding genes ($p$ = 1.56e-6), and windows that did not include any of these features ($p$ = 5.02e-14; Fig. 5B) while decaying at roughly equivalent rates as these features with increasing genomic distance (Fig. 5A). We also find that the 10kb windows centered on most features differ in how similar they are to the species tree as inferred from coding genes or UCEs alone. All features except recombination hotspots are more similar to the species tree on average than windows that contain no features, while UCEs are more similar to the species tree than when compared to any other feature (Fig. 5C).

*Consequences of tree misspecification on analyses of molecular evolution*

Next, we examined how phylogenetic discordance influenced inferences on the evolution of protein-coding sequences. Among a set of 22,261 *M. musculus* protein-coding transcripts, the average distance between the start and end of the coding sequence was 37.02 kb, or roughly 4 non-overlapping 10 kb windows. At this distance, tree similarity is predicted to diminish considerably (*e.g.*, by 0.10 wRF units), such that the phylogenetic history of individual genes may often contain some phylogenetic discordance (Mendes and Hahn 2016; Mendes et al. 2019). We also found that out of the 67,566 times the coding sequence in a gene overlapped with a 10 kb window, the inferred topology of the gene tree exactly matched the topology of the corresponding window tree only 11% of the time. Thus, the common practice of inferring gene trees on concatenated coding exons from a single transcript is still likely averaging over multiple possible histories.

Finally, we tested how tree misspecification might impact standard $d_N/d_S$ based phylogenetic analyses for positive directional selection. Specifically, we used the common practice of assuming a single species tree for all genes and compared that to using individually inferred gene trees in three common statistical tests for positive selection: PAML's M1a vs. M2a test (Yang 2007), HyPhy's BUSTED test (Murrell et al. 2015), and HyPhy's aBSREL test (Smith et al. 2015a). We found evidence that tree misspecification likely induces both false positive (type I) and false negative (type II) errors. For example, many genes were inferred as having experienced positive directional selection when using a single species tree, but not when using local gene trees and vice versa (Fig. 6A). Assuming the locally inferred gene tree is more accurate, this resulted in varying rates and types of error (Table 5). For BUSTED, we observe that 28% of genes inferred as having evolved under positive directional selection when using the gene tree were not inferred when using the concatenated species tree (likely false negatives). The opposite was true for M1a vs. M2a, where, among genes showing inconsistent evidence for positive selection across the two scenarios, 76% do so when using the concatenated species tree but not individual gene trees (likely false positives). In general, genes found to be evolving under positive selection using both tree types tended to be more concordant with the species tree than those that had evidence for positive selection either using only the concatenated tree or the gene tree (Fig. 6).

## Discussion

Phylogenies provide insight into the relationships of species and serve as a framework for asking questions about molecular and trait evolution. However, phylogenetic histories can vary extensively across regions of a genome, and evolutionary relationships between species may not often be well represented by a single representative species-level phylogeny. Here, we combine the resources of the house mouse (*Mus musculus*) with new and recently published (Kumon et al. 2021) genomes from seven species to understand the systematics of murine rodents and causes and consequences of phylogenetic discordance along murine genomes. These new analyses help to place this important model system in a stronger evolutionary context and begin to fill the gap in sampling of murine rodents which, despite their exceptional morphological and ecological diversity and species richness, have had relatively few whole genomes sequenced. They further provide us with the resources to study the landscape of phylogenetic discordance across the

genome, understand how recombination and natural selection shape phylogenetic histories, and evaluate how assuming a single evolutionary history can compromise the study of molecular evolution. Beyond studying the patterns of discordance, this work highlights the importance of a nuanced molecular evolution analysis in a biomedical model system.

*Phylogenomic relationships of murine rodent lineages from conserved genomic regions*

The extraordinary species richness of murine rodents complicates phylogenetic analyses because of the resources required to sample, sequence, and analyze such widely distributed taxa. Earlier work either attempted to resolve specific groups such as *Mus* (Lundrigan et al. 2002; Suzuki et al. 2004) and *Apodemus* (Serizawa et al. 2000; Liu et al. 2004), or to uncover broader relationships across the subfamily (Martin et al. 2000; Steppan et al. 2005). In both cases, a limited number of nuclear or mitochondrial genes were used. Even so, evidence from these datasets suggested phylogenetic discordance across Murinae, including between mitochondrial and nuclear genes, that lead to different genomic regions supporting incompatible phylogenetic reconstructions (Suzuki et al. 2004; Steppan et al. 2005; White et al. 2009). Lecompte et al. (2008) provided one of the earliest well-supported phylogenetic reconstructions from across Murinae and the tribal classifications they proposed remain generally supported. More recent work has increased the number of taxa sampled, both for analyses of Murinae specifically (Pagès et al. 2016) and for their placement within Muridae and Muroidea (Schenk et al. 2013; Steppan and Schenk 2017; Rowe et al. 2019), but the number of loci used for phylogenetic inference remained limited to six loci or fewer. Recent work focused on Hydromyini made use of substantially more loci (1,245 exons, (Roycroft et al. 2020) 1,360 exons, (Roycroft et al. 2021) exons for phylogenetic reconstruction.

Here we reconstructed a species tree of murine rodents based on 2,632 UCEs from 18 species across the radiation. The inferred tree (Fig. 1) is topologically consistent with those inferred in previous studies (Lecompte et al. 2008; Steppan and Schenk 2017; Aghova et al. 2018). Branch support was uniformly high, and gene trees unambiguously support the tribal classification of Lecompte et al. (2008). However, four shorter branches show more substantial gene tree discordance (Fig. 1, branches D, E, H, and J), with two recovered clades (E and J) being supported by less than half of all gene trees. We also estimated divergence times on our inferred species tree using four fossil calibration points (Table 2), recovering times that are roughly consistent with the relatively young estimates found by (Steppan and Schenk 2017) (see Supplement).

*The genomic landscape of phylogenetic discordance*

Limiting the number and nature of the loci used to resolve species relationships is often useful to get a clear picture of the species' history across many taxa. However, such targeted approaches may fail to capture the degree of discordance driven by a combination of incomplete lineage sorting and introgression (Alexander et al. 2017; Chan et al. 2020; Vanderpool et al. 2020; Alda et al. 2021). Our results highlighted these limitations and the general relationships between phylogenetic patterns and functional attributes of the genome in several interesting ways. Using

resources from the *M. musculus* model system, we found that the species tree inferred from genes or UCEs was not the most common topology recovered across the genome and did not match evolutionary relationships inferred for over 85% of the genome. This result was driven mainly by discordance among three more closely related (Praomyini) species sampled for this study, which had the lowest gCF and second lowest sCF in the UCE species tree (Fig 1, node J). In the window analysis, each alternate topology of this clade occurred at a frequency of roughly 14% while the rest of the topology remained consistent with the species tree (Fig. 2). The equal frequencies of the alternate topologies of the Praomyini clade along the chromosome suggest that incomplete lineage sorting is the cause of this discordance. Although similar frequencies were observed among these three most common trees, it is noteworthy that the topology robustly inferred from genes or UCEs was not that common overall and only the third most frequent topology among 10kb windows across the entire genome. This underscores that while a single inferred species tree may be of general interest when reconstructing the speciation history of a group, individual locus trees are likely to be more accurate when making inferences about the evolution of particular regions or features of the genome.

While we observed no clear clustering of topological structures along most chromosomes (*e.g.*, Fig. 3C), we found that this enormous range of phylogenetic variation was not randomly distributed within chromosomes. Perhaps surprisingly, we did not observe a relationship between local recombination rates in mice (*M. musculus*) and the degree of local phylogenetic discordance, suggesting that recombination rate may often evolve sufficiently quickly that contemporary estimates do not track variation over deeper evolutionary. Similar to findings in Great Apes (Hobolth et al. 2007), these results suggest that even high-resolution genetic resources from a single model species may be insufficient to help predict the local landscape of discordance in a phylogenetic sample spanning over 12 million years of evolution. This stands in contrast to the well-known negative relationship between population-level nucleotide variation and recombination rates in several mammals (Cai et al. 2009; Corbett-Detig et al. 2015), including in house mouse (Cai et al. 2009; Geraldes et al. 2011; Corbett-Detig et al. 2015; Kartje et al. 2020). However, we did find a positive correlation between recombination rate and discordance with the inferred species tree, in line with previous work in primates (Pease and Hahn 2013; Rivas-Gonzalez et al. 2023), placental mammals (Foley et al. 2023) and *Drosophila* (Pease and Hahn 2013).

One source of evolution in the recombination map may be changes in synteny. Our reference-guided analyses assume collinearity between *Mus* and the other lineages we are comparing (*i.e.*, no karyotype variation), at least at the window-based scale we are comparing variation. Structural variation, including substantial variation in chromosome numbers, are likely to be widespread in rodents (Stanyon et al. 1999; Yalcin et al. 2011; Romanenko et al. 2012; Keane et al. 2014) and has the potential to skew our results when comparing tree similarity between regions of the genome using multiple species. Generating chromosome-scale assemblies for many non-*Mus* and *Rattus* species may prove limiting given that most tissue resources for this group are derived from natural history collections that often lack high molecular weight DNA. Nonetheless,

whole genome alignments between mouse and rat indicate high degrees of chromosomal synteny and co-linearity (Fig S6), suggesting that many regions will be colinear in our sample.

Natural selection reduces the effective population size ($N_e$) of genomic regions through the processes of genetic hitchhiking of variation linked to the fixation of positively selected mutations (*i.e.*, selective sweeps; Smith and Haigh 1974; Kaplan et al. 1989) and the purging of deleterious mutations (*i.e.*, background selection; Charlesworth et al. 1993; Hudson and Kaplan 1995). Thus, variation on parameters dependent on $N_e$ – such as standing levels of nucleotide variation and patterns of incomplete lineage sorting – should be influenced by linkage to functional elements. Consistent with this general prediction, we observed less gene tree/species tree discordance near protein-coding genes (Fig. 5C), similar to previous results (Scally et al. 2012; Rivas-Gonzalez et al. 2023), as well as other features like UCEs and recombination hotspots. We also assessed local phylogenetic discordance in 10kb windows around these genomic features and found varying degrees of phylogenetic similarity, presumably reflecting variation in the strength and frequency of linked selection over time (Fig. 5A and B). For instance, regions immediately adjacent to recombination hotspots are, on average, more similar than regions around no genomic features (Fig. 5B), and this similarity is retained over long distances (up to 5Mb; Fig. 5A).

The regions immediately adjacent to UCEs are significantly more similar than regions not near any of the genomic features we considered, and this similarity dissipated at rates similar to chromosome-wide levels. Notably, this pattern is consistent when comparing regions around UCEs to any of the other genomic features we studied. These results suggest that a history of strong purifying selection on UCEs (Katzman et al. 2007) more generally strongly skews patterns of discordance consistent with a persistent local reduction in $N_e$. One practical consequence of this is that phylogenetic inferences based on UCE markers would seem less prone to discordance and may provide cleaner estimates of species tree history than randomly chosen regions. Indeed, windows centered on UCEs have a higher degree of similarity to the species tree than other genomic features (i.e., 17% concordance with the species tree, versus 13% genome-wide or 15% for protein-coding genes). However, it is worth noting that UCEs are also more likely to provide a skewed and potentially misleading underestimate genome-wide levels of discordance. Given this relationship, inferences based on UCEs may not, for example, be extended to related phylogenetic parameters of interest (*e.g.*, ancestral population sizes), and, despite the relative ease of generating UCE data, such markers are not suitable for genetic inferences within populations. Our data suggest that background selection is important in structuring variation due to incomplete lineage sorting.

*Discordance and Molecular Evolution*

We also found that the choice of tree topology drastically affects the results from various common tests for positive selection. It is known that tree misspecification can lead to incorrect placement of substitutions on branches, possibly leading to spurious results for tests of positive directional selection (Hahn and Nakhleh 2016; Mendes and Hahn 2016). Here, we show that these errors result

592 in false positive (detected signal for selection only when using the gene tree) and false negative
593 results (detected signal for selection only when using the species tree).
594 For each of three selection tests run, HyPhy's BUSTED and aBSREL and PAML's M1a
595 vs. M2a some genes showed evidence of positive selection whether the species tree or gene tree
596 was used while many other genes had signatures of positive selection restricted only to a single
597 tree. The genes unique to the type of tree used were often discordant with the species tree. In
598 contrast, the genes that showed evidence of positive selection regardless of tree had levels of
599 discordance comparable to all genes (85%, Fig. 6, numbers in parentheses). This suggests that mis-
600 mapping substitutions by supplying these tests with the wrong tree (*i.e.*, the species tree when gene
601 trees are discordant) can lead to inflated false positive and false negative rates when inferring genes
602 under positive selection. The magnitude and direction of these biases were dependent on the
603 underlying model. So-called branch-site models that allow substitution rates to vary among both
604 branches and codon sites, such as HyPhy's BUSTED and aBSREL models, resulted in more genes
605 inferred with evidence for positive selection when using the inferred gene tree (*i.e.*, the correct
606 tree, assuming no errors in gene tree reconstruction). This means that using a single species tree
607 for these tests reduces the power to detect positive selection. On the other hand, models that only
608 allow rates to vary among sites, such as PAML's M1a vs. M2a test, showed an increase in the
609 number of putative false positives inferred when using the wrong tree. That is, tree mis-
610 specification results in spurious increases in $d_N/d_S$ that mimic positive selection.
611 These results have wide-ranging implications for phylogenetics and comparative genomic
612 analysis. First, it is imperative that when testing a specific locus for positive selection, discordance
613 among loci must be accounted for. This is most easily achieved by simply using the gene tree (or
614 other locus type) as input to the test for selection (Good et al. 2013; Mendes and Hahn 2016;
615 Roycroft et al. 2021). However, as Mendes and Hahn (2016) pointed out, this may not completely
616 mask the effects of discordance on substitution rates, as sites within a single gene may still have
617 evolved under different histories because of within-gene recombination. We also find evidence for
618 this here, given that tree similarity diminished at scales that were less than the average genomic
619 distance between the beginning and end of a coding sequence in mice (37.02 kb in this data set).
620 Nevertheless, starting with an inferred gene tree is advisable whenever possible, followed by a
621 secondary analysis of evidence for within-gene variation in phylogenetic history. However,
622 incorporating discordance into a comparative framework is not trivial and many comparative
623 genomic methods assume a single species tree that test for changes in substitution rates in a
624 phylogeny (Pollard et al. 2010; Hu et al. 2019; Partha et al. 2019). Even methods that allow the
625 use of different trees for different loci (like PAML and HyPhy) are still commonly applied with a
626 single species tree across loci (Carbone et al. 2014; Foote et al. 2015; van der Valk et al. 2021;
627 Treaster et al. 2023). Our results confirm that the use of a single tree for such tests that rely on
628 accurate estimation of substitution rates are likely to lead to both false negative and false positive
629 inferences of positive selection.
630 Finally, because of recombination's underlying contribution to phylogenomic discordance,
631 one might be tempted to control for alternate topologies in a comparative genomic dataset by using

a genetic map from a single, well-studied species and sampling regions with low recombination rates. However, our results show that using a single recombination map is insufficient to control for discordance even among a small sample of seven species. This is likely because the recombination rate also evolves and is linked to structural variation (Morgan et al. 2017) which is unaccounted for with use of a single reference genome, resulting in a diminished correlation signal between rates and phylogenetic discordance over time. This would likely be compounded for more species spanning deeper evolutionary timescales.

**Acknowledgments**

We thank Jake Esselstyn and Kevin Rowe for helpful comments and discussion on the murine species tree and Matt Hahn and the Hahn lab for feedback on the manuscript. We also thank Brant Faircloth and Trevor Sless for advice on using phyluce. We are grateful for tissue samples provided by Chris Conroy at the Museum of Vertebrate Zoology, Berkeley, CA (MVZ) and Adam Ferguson at the Field Museum of Natural History, Chicago, IL (FMNH), and to the original collectors. This work was supported by the National Science Foundation (DEB-1754096 to J.M.G), the Eunice Kennedy Shriver National Institute of Child Health and Human Development of the National Institutes of Health (R01-HD094787 to J.M.G.). J.J.H. received financial support from the Cornell Center for Vertebrate Genomics. J. S. B. was supported by the University of Michigan Life Sciences Fellows Program and the Jean Wright Cohn Endowment Fund at the University of Michigan Museum of Zoology. Computations for species tree reconstruction were performed using the computer clusters and data storage resources of the University of California Riverside HPCC, which were funded by grants from NSF (MRI-2215705, MRI-1429826) and NIH (1S10OD016290-01A1), and the Cornell University Biotechnology Resource Center BioHPC (RRID:SCR_021757) with help from Qi Sun. Bioinformatic analyses for genomic discordance and selection tests were conducted using the University of Montana Griz Shared Computing Cluster supported by grants from the NSF (CC-2018112 and OAC-1925267, J.M.G. co-PI). Any opinions, findings, and conclusions or recommendations expressed in this material are those of the authors and do not necessarily reflect the views of the NSF or the NIH.

**Data availability**

For the six previously assembled genomes (see Table 1), all raw reads and assemblies are available as an NCBI BioProject (Accession Number PRJNA669840). The reads and assembly for *Otomys* typus, pseudo-assemblies for the six other new samples, and locus alignments (UCEs, genes, and genomic windows) are available on Dryad (https://doi.org/10.5061/dryad.866t1g1wq). All code and summary data for this project are deposited on github (https://github.com/gwct/murine-discordance).

## Tables

**Table 1: All taxa whose genomes were included in this study, the source of the assembly, and the assembly level of each genome. For the six samples used in the genome-wide discordance analyses (column 5, except for mm10), we also generated reference-based pseudo-assemblies using the mouse genome (mm10) as the reference.**

| Taxon | Assembly source | Assembly level | No. UCEs | Used in genome-wide discordance analyses |
|---|---|---|---|---|
| *Apodemus speciosus* | GenBank: GCA_002335545.1 | Scaffolds | 2336 | |
| *Apodemus sylvaticus* | GenBank: GCA_001305905.1 | Scaffolds | 2510 | |
| *Arvicanthis niloticus* | GenBank: GCA_011762505.1 | Chromosomes | 2563 | |
| *Grammomys dolichurus* | Kumon et al., 2021: *de novo* assembled | Chromosomes | 2395 | * |
| *Hylomyscus alleni* | Kumon et al., 2021: *de novo* assembled | Chromosomes | 2392 | * |
| *Mastomys natalensis* | Kumon et al., 2021: *de novo* assembled | Chromosomes | 2483 | * |
| *Mus caroli* | GenBank: GCA_900094665.2 | Chromosomes | 2584 | |
| *Mus musculus* | GenBank: GRCm38.p6/mm10 | Chromosomes | 2294 | * |
| *Mus pahari* | GenBank: GCA_900095145.2 | Chromosomes | 2556 | |
| *Mus spretus* | GenBank: GCA_001624865.1 | Chromosomes | 2578 | |
| *Otomys typus* | This study: *de novo* assembled | Scaffolds | 2627 | |
| *Phodopus sungorus* | Moore et al., 2022: *de novo* assembled | Chromosomes | 2633 | |
| *Praomys delectorum* | Kumon et al., 2021: *de novo* assembled | Chromosomes | 2549 | * |
| *Rattus norvegicus* | GenBank: GCA_015227675.2 | Chromosomes | 2425 | |
| *Rattus rattus* | GenBank: GCA_011064425.1 | Chromosomes | 2443 | |
| *Rhabdomys dilectus* | Kumon et al., 2021: *de novo* assembled | Chromosomes | 2546 | * |
| *Rhombomys opimus* | GenBank: GCA_010120015.1 | Scaffolds | 2627 | |
| *Rhynchomys soricoides* | Kumon et al., 2021: *de novo* assembled | Chromosomes | 2570 | * |

678

679 **Table 2: Prior node ages used in phylogenetic dating in millions of years before present.**

| Clade | Minimum Age | Maximum Age | Citation |
|---|---|---|---|
| *Mus* | 5.3 | 7.2 | Steppan and Schenk, 2017 |
| *Apodemus* | 5.3 | 7.2 | Schenk et al., 2013 |
| *Rattus* | 2.4 | 3.6 | Steppan and Schenk, 2017 |
| Murinae | 12.1 | 14.05 | Schenk et al., 2013 |

680

681 **Table 3: The most frequently recovered topologies across all 10kb windows. RS = *Rhyncomys***
682 ***soricoides*, GD = *Grammomys dolichurus*, RD = *Rhabdomys dilectus*, MM = *Mus musculus*,**
683 **HA = *Hylomyscus alleni*, MN = *Mastomys natalensis*, PD = *Praomys delectorum*.**

| Rank | Topology | # of windows | Proportion of windows |
|---|---|---|---|
| 1 | (RS,((GD,RD),(MM,((HA,MN),PD)))); | 23864 | 0.146 |
| 2 | (RS,((GD,RD),(MM,((HA,PD),MN)))); | 23836 | 0.146 |
| 3* | (RS,((GD,RD),(MM,(HA,(MN,PD))))); | 21509 | 0.131 |
| 4 | (RS,(MM,((GD,RD),((HA,MN),PD)))); | 14417 | 0.088 |
| 5 | (RS,(MM,((GD,RD),((HA,PD),MN)))); | 14321 | 0.0874 |
| 6 | (RS,(MM,((GD,RD),(HA,(MN,PD))))); | 14044 | 0.0858 |
| 7 | (RS,(((HA,PD),MN),(MM,(GD,RD)))); | 11723 | 0.0716 |
| 8 | (RS,(((HA,MN),PD),(MM,(GD,RD)))); | 11308 | 0.0691 |

684 *The topology recovered from concatenation of genes or UCEs

685 **Table 4: Summaries of phylogenies per chromosome.**

| Chromosome | # of unique topologies recovered |
|---|---|
| 1 | 184 |
| 2 | 123 |
| 3 | 114 |
| 4 | 144 |
| 5 | 134 |
| 6 | 172 |
| 7 | 218 |
| 8 | 133 |
| 9 | 116 |
| 10 | 110 |
| 11 | 93 |
| 12 | 179 |
| 13 | 186 |
| 14 | 173 |

| | |
|---|---|
| 15 | 96 |
| 16 | 94 |
| 17 | 188 |
| 18 | 75 |
| 19 | 82 |
| X | 207 |

686

687 **Table 5: Rates and types of error when using concatenated trees for gene-based selection**
688 **tests.**

| Test | False positive rate | False negative rate |
|---|---|---|
| BUSTED | 0.45% | 28.10% |
| aBSREL | 0.41% | 10.60% |
| M1a vs. M2a | 2.66% | 3.20% |

689

690

691

## Figures

### Figure 1

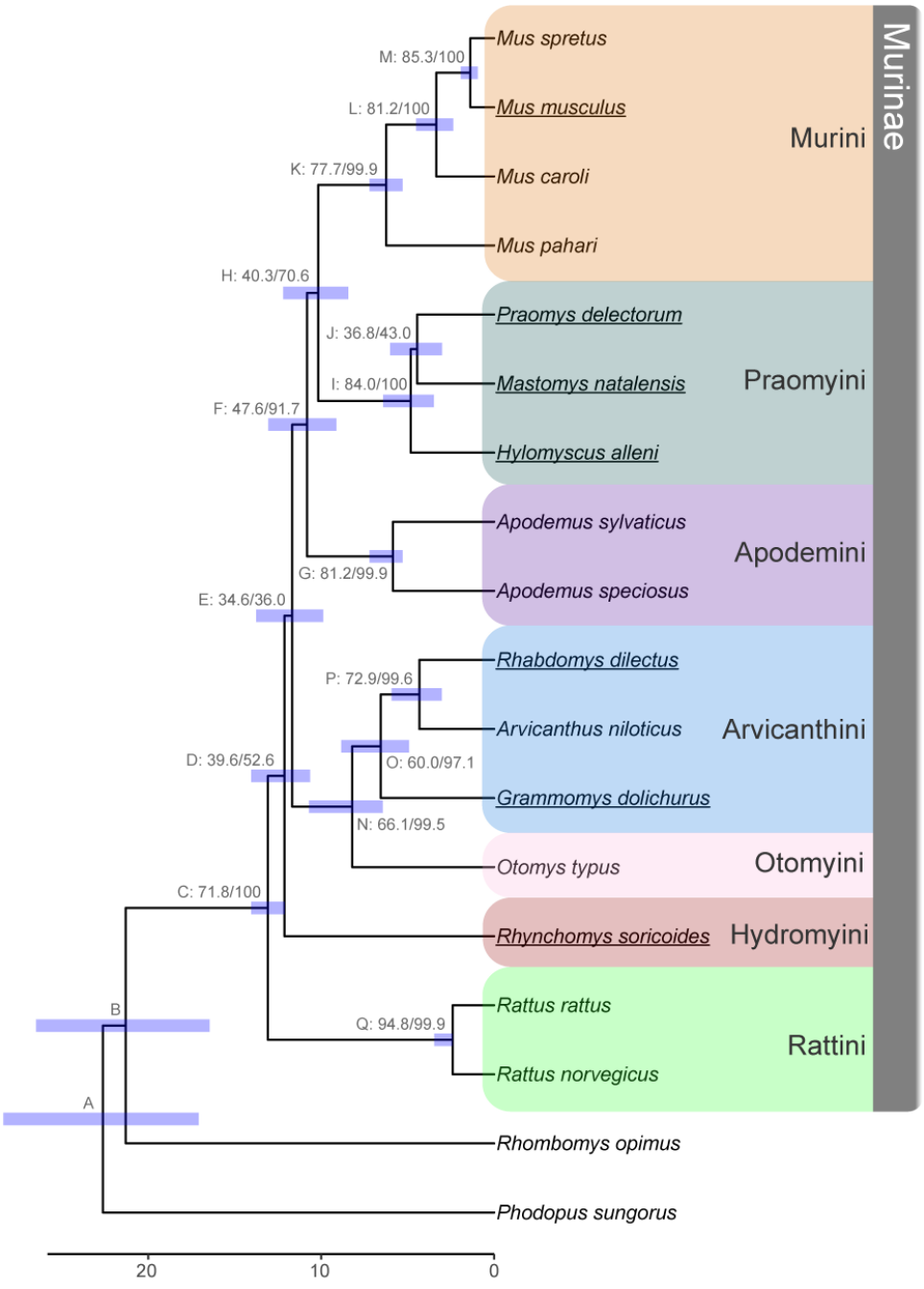


**Figure 1:** Species trees inferred from concatenation of ultra-conserved elements (UCEs) from 18 rodent species. Internal nodes are labeled by a letter identifier referenced in the text and site and gene concordance factors (*i.e.*, Label: sCF/gCF) as well as a bar indicating the confidence interval for divergence time estimation. Ultrafast bootstrap/SH-aLRT values were all 100. Bottom scale represents time in millions of years before present. Fossil calibrations are described in Tables 2

700 and S2, with node C used as a fixed calibration point. Tribes within sub-family Murinae are
701 highlighted on the right following the classifications used by Lecompte et al. (2008). Genomes
702 used for the genome-wide phylogenetic discordance analyses are underlined.

703

**Figure 2**

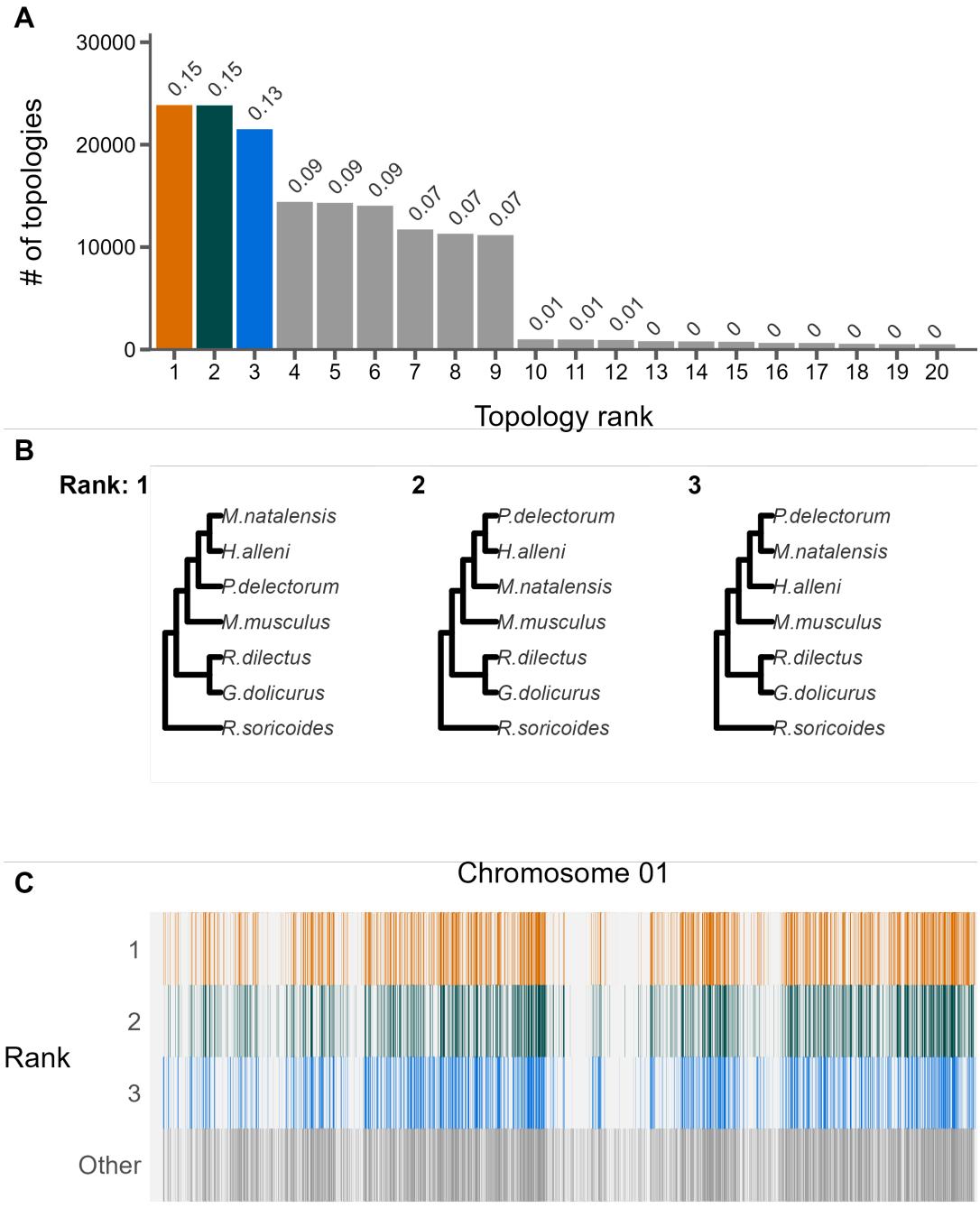


**Figure 2:** The landscape and profile of phylogenetic discordance across non-overlapping 10kb windows in murine genomes. A) Distribution of the 20 most frequent topologies recovered across all windows. Numbers above bars indicate proportion of each topology. B) The top three topologies recovered across all chromosomes 1. C) Distribution of the topologies recovered along

chromosome 1. The x-axis is scaled to the length of the chromosome and each vertical bar represents one 10kb window. The three most frequent topologies occupy the first three rows while all other topologies are shown in the bottom row. See Supplemental File S1 for individual chromosome plots.

**Figure 3**

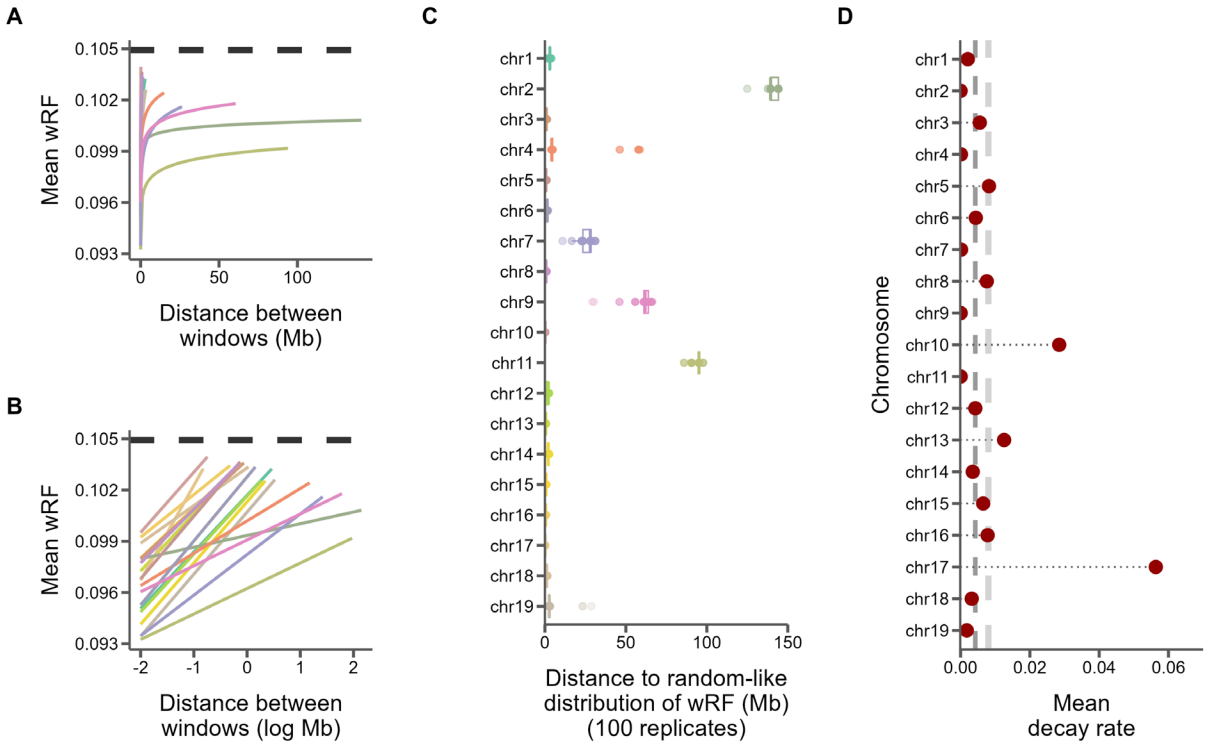


**Figure 3:** Similarity between 10kb windows decays as genomic distance between windows increases. A) The log fit to the mean of distributions of weighted Robinson-Foulds distances between trees of windows at increasing genomic distance (10kb steps). Each line represents one chromosome. B) The same, but on a log scale with a linear fit. C) For every window on each chromosome, the genomic distance between windows at which tree distance becomes random for 100 replicates of random window selection. D) The slopes of the correlation between genomic distance and tree distance from panel B represent the rate at which tree similarity decays across the genome.

**Figure 4**

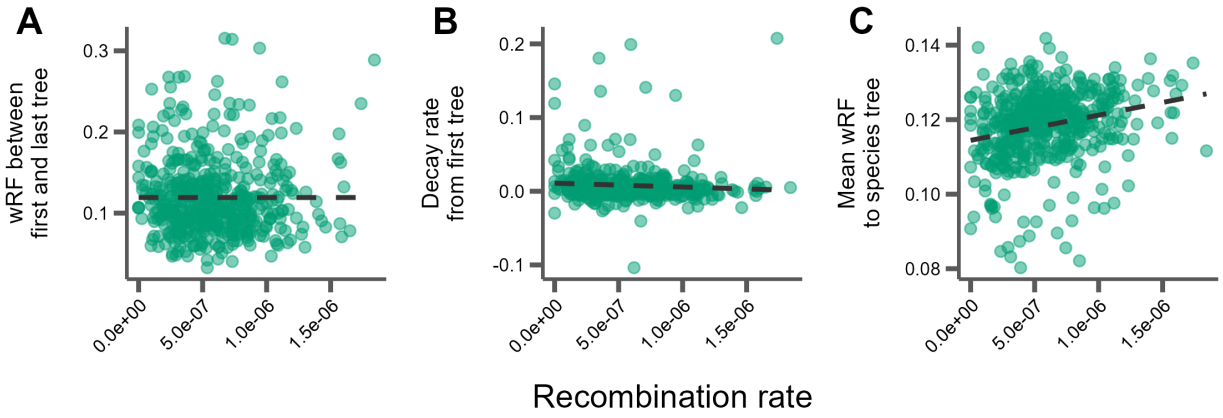


**Figure 4:** Correlations between tree similarity and recombination rate in 5Mb windows. A) Tree similarity as measured by the weighted Robinson-Foulds distance between the first and last 10kb windows within the 5Mb window. B) The slopes of the linear correlation between the weighted Robinson-Foulds distances between the first 10kb window and every other 10kb window within a 5Mb window represent the rate at which tree similarity decays over each 5Mb window. C) The mean wRF of all 10kb window trees within each 5Mb window compared to the species tree.

735 **Figure 5**

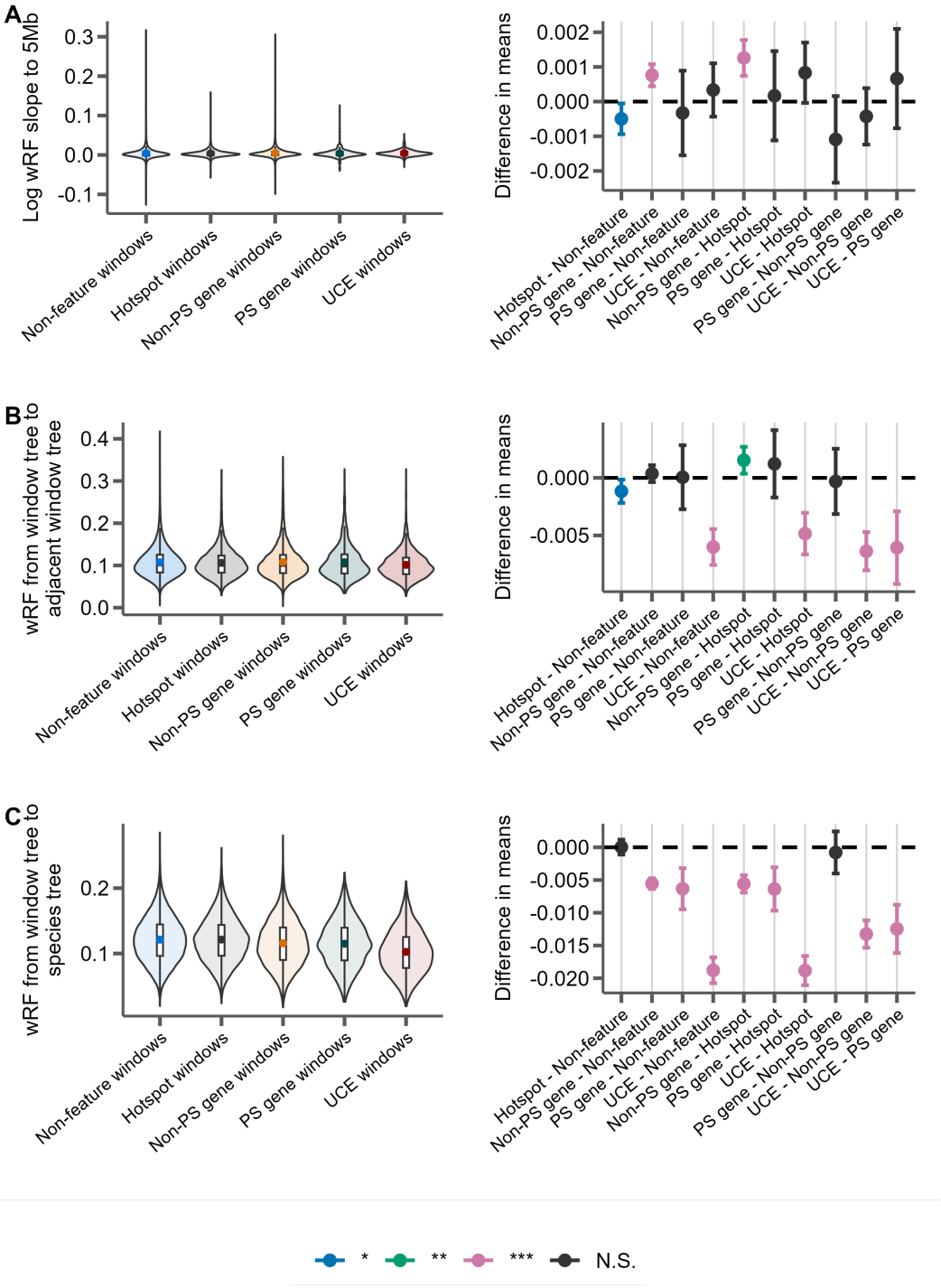


736

737 **Figure 5:** Distributions of weighted Robinson-Foulds distance from trees constructed from 10kb
738 windows either centered on recombination hotspots (Hotspot), protein-coding genes without
739 evidence for positive selection (Non-PS genes), protein coding genes with evidence for positive

selection (PS genes), UCEs, or containing none of these features (Non-feature). For each panel, the left portion shows the distributions of the measure for each feature type and the right panel shows the differences in means for each pairwise comparison of features with significance assessed with Tukey's range test. The labels on the x-axis indicate the feature pairs being compared, with the first feature being the reference (*i.e.* points above 0 indicate this feature has a higher mean). *P*-value thresholds: * < 0.05, ** < 0.01, *** <0.001. A) The rate of decay of phylogenetic similarity is calculated as the slope of a linear regression between wRF and the log distance between each window up to 5Mb away from the feature window. B) The phylogenetic similarity of windows immediately adjacent to feature windows. C) The phylogenetic similarity between the species tree inferred from protein-coding gene trees and the feature window.

751 **Figure 6**

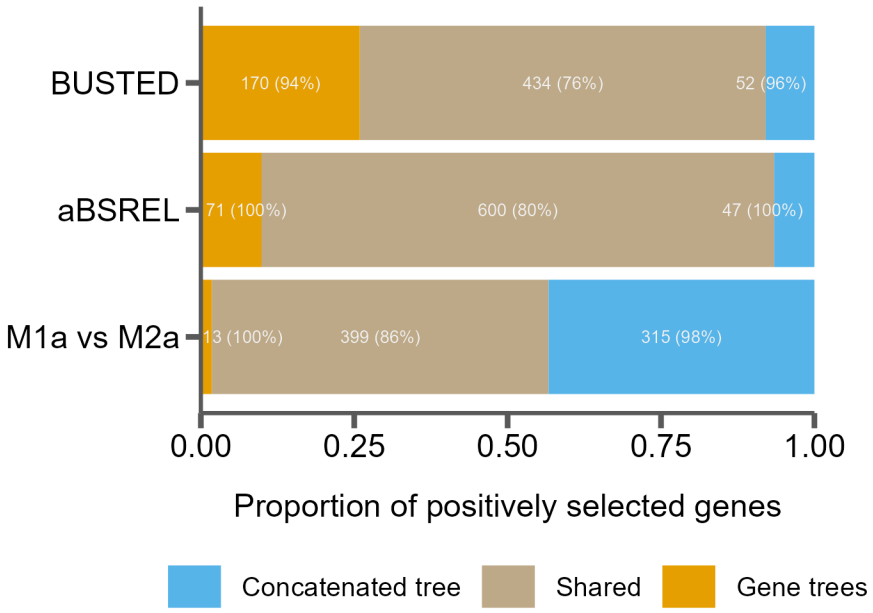


752

753 **Figure 6:** Tree misspecification leads to erroneous results in tests for positive selection. The
754 proportion of genes inferred to be under positive selection for three tests using either a single
755 species tree (concatenated tree) or individual gene trees, as well as those found in both cases
756 (shared). Numbers in the bars indicate raw counts, and percentages indicate the percent of genes
757 in that category that are discordant from the species tree.

758

759

760

## References


Pdb (the paleobiology database) [Internet]. 2011 January 21st, 2022]. Available from: http://paleodb.org/

Aghova T, Kimura Y, Bryja J, Dobigny G, Granjon L, Kergoat GJ. 2018. Fossils know it best: Using a new set of fossil calibrations to improve the temporal phylogenetic framework of murid rodents (Rodentia: Muridae). *Mol Phylogenet Evol*. 128:98-111.

Alda F, Ludt WB, Elias DJ, McMahan CD, Chakrabarty P. 2021. Comparing ultraconserved elements and exons for phylogenomic analyses of Middle American cichlids: When data agree to disagree. *Genome Biol Evol*. 13:evab161.

Alexander AM, Su YC, Oliveros CH, Olson KV, Travers SL, Brown RM. 2017. Genomic data reveals potential for hybridization, introgression, and incomplete lineage sorting to confound phylogenetic relationships in an adaptive radiation of narrow-mouth frogs. *Evolution*. 71:475-488.

Avise JC, Robinson TJ. 2008. Hemiplasy: A new term in the lexicon of phylogenetics. *Syst Biol*. 57:503-507.

Baum DA. 2007. Concordance trees, concordance factors, and the exploration of reticulate genealogy. *Taxon*. 56:417-426.

Benjamini Y, Hochberg Y. 1995. Controlling the false discovery rate: A practical and powerful approach to multiple testing. *Journal of the Royal statistical society: series B (Methodological)*. 57:289-300.

Bloom BH. 1970. Space/time trade-offs in hash coding with allowable errors. *Commun. ACM*. 13:422–426.

Böcker S, Canzar S, Gunnar WK. 2013. The generalized Robinson-Foulds metric. In: Darling A, Stoye J, editors. Algorithms in bioinformatics. Berlin, Heidelberg: Springer.

Bolger AM, Lohse M, Usadel B. 2014. Trimmomatic: A flexible trimmer for Illumina sequence data. *Bioinformatics*. 30:2114-2120.

Borowiec ML. 2016. Amas: A fast tool for alignment manipulation and computing of summary statistics. *PeerJ*. 4:e1660.

Bradley RK, Roberts A, Smoot M, Juvekar S, Do J, Dewey C, Holmes I, Pachter L. 2009. Fast statistical alignment. *PLoS Comput Biol*. 5:e1000392.

Cai JJ, Macpherson JM, Sella G, Petrov DA. 2009. Pervasive hitchhiking at coding and regulatory sites in humans. *PLoS Genet*. 5:e1000336.

Capella-Gutierrez S, Silla-Martinez JM, Gabaldon T. 2009. Trimal: A tool for automated alignment trimming in large-scale phylogenetic analyses. *Bioinformatics*. 25:1972-1973.

Carbone L, Harris RA, Gnerre S, Veeramah KR, Lorente-Galdos B, Huddleston J, Meyer TJ, Herrero J, Roos C, Aken B, et al. 2014. Gibbon genome and the fast karyotype evolution of small apes. *Nature*. 513:195-201.

Chan KO, Hutter CR, Wood PL, Jr., Grismer LL, Brown RM. 2020. Target-capture phylogenomics provide insights on gene and species tree discordances in Old World treefrogs (Anura: Rhacophoridae). *Proc Biol Sci*. 287:20202102.

Charlesworth B, Morgan MT, Charlesworth D. 1993. The effect of deleterious mutations on neutral molecular variation. *Genetics*. 134:1289-1303.

Chernomor O, von Haeseler A, Minh BQ. 2016. Terrace aware data structure for phylogenomic inference from supermatrices. *Syst Biol*. 65:997-1008.

Christmas MJ, Kaplow IM, Genereux DP, Dong MX, Hughes GM, Li X, Sullivan PF, Hindle AG, Andrews G, Armstrong JC, et al. 2023. Evolutionary constraint and innovation across hundreds of placental mammals. *Science*. 380:eabn3943.

Corbett-Detig RB, Hartl DL, Sackton TB. 2015. Natural selection constrains neutral diversity across a wide range of species. *PLoS Biol*. 13:e1002112.

Cox A, Ackert-Bicknell CL, Dumont BL, Ding Y, Bell JT, Brockmann GA, Wergedal JE, Bult C, Paigen B, Flint J, et al. 2009. A new standard genetic map for the laboratory mouse. *Genetics*. 182:1335-1344.

Cunningham F, Allen JE, Allen J, Alvarez-Jarreta J, Amode MR, Armean IM, Austine-Orimoloye O, Azov AG, Barnes I, Bennett R, et al. 2022. Ensembl 2022. *Nucleic Acids Res*. 50:D988-D995.
Danecek P, Bonfield JK, Liddle J, Marshall J, Ohan V, Pollard MO, Whitwham A, Keane T, McCarthy SA, Davies RM, Li H. 2021. Twelve years of samtools and bcftools. *Gigascience*. 10: giab008.
Degnan JH, Rosenberg NA. 2006. Discordance of species trees with their most likely gene trees. *PLoS Genet*. 2:e68.
Edwards SV. 2009. Is a new and general theory of molecular systematics emerging? *Evolution*. 63:1-19.
Faircloth BC. 2013. Illumiprocessor: A trimmomatic wrapper for parallel adapter and quality trimming.
Faircloth BC. 2016. Phyluce is a software package for the analysis of conserved genomic loci. *Bioinformatics*. 32:786-788.
Faircloth BC, McCormack JE, Crawford NG, Harvey MG, Brumfield RT, Glenn TC. 2012. Ultraconserved elements anchor thousands of genetic markers spanning multiple evolutionary timescales. *Syst Biol*. 61:717-726.
Feng S, Bai M, Rivas-Gonzalez I, Li C, Liu S, Tong Y, Yang H, Chen G, Xie D, Sears KE, et al. 2022. Incomplete lineage sorting and phenotypic evolution in marsupials. *Cell*. 185:1646-1660.
Foley NM, Mason VC, Harris AJ, Bredemeyer KR, Damas J, Lewin HA, Eizirik E, Gatesy J, Karlsson EK, Lindblad-Toh K, et al. 2023. A genomic timescale for placental mammal evolution. *Science*. 380:eabl8189.
Fontaine MC, Pease JB, Steele A, Waterhouse RM, Neafsey DE, Sharakhov IV, Jiang X, Hall AB, Catteruccia F, Kakani E, et al. 2015. Mosquito genomics. Extensive introgression in a malaria vector species complex revealed by phylogenomics. *Science*. 347:1258524.
Foote AD, Liu Y, Thomas GW, Vinar T, Alfoldi J, Deng J, Dugan S, van Elk CE, Hunter ME, Joshi V, et al. 2015. Convergent evolution of the genomes of marine mammals. *Nat Genet*. 47:272-275.
Gable SM, Byars MI, Literman R, Tollis M. 2022. A genomic perspective on the evolutionary diversification of turtles. *Syst Biol*. 71:1331-1347.
Geraldes A, Basset P, Smith KL, Nachman MW. 2011. Higher differentiation among subspecies of the house mouse (Mus musculus) in genomic regions with low recombination. *Mol Ecol*. 20:4722-4736.
Gibbs RA, Weinstock GM, Metzker ML, Muzny DM, Sodergren EJ, Scherer S, Scott G, Steffen D, Worley KC, Burch PE, et al. 2004. Genome sequence of the brown Norway rat yields insights into mammalian evolution. *Nature*. 428:493-521.
Good JM, Wiebe V, Albert FW, Burbano HA, Kircher M, Green RE, Halbwax M, Andre C, Atencia R, Fischer A, Paabo S. 2013. Comparative population genomics of the ejaculate in humans and the great apes. *Mol Biol Evol*. 30:964-976.
Green RE, Krause J, Briggs AW, Maricic T, Stenzel U, Kircher M, Patterson N, Li H, Zhai W, Fritz MH, et al. 2010. A draft sequence of the Neandertal genome. *Science*. 328:710-722.
Guindon S, Dufayard JF, Lefort V, Anisimova M, Hordijk W, Gascuel O. 2010. New algorithms and methods to estimate maximum-likelihood phylogenies: Assessing the performance of phyml 3.0. *Syst Biol*. 59:307-321.
Hahn MW, Nakhleh L. 2016. Irrational exuberance for resolved species trees. *Evolution*. 70:7-17.
He B, Zhao Y, Su C, Lin G, Wang Y, Li L, Ma J, Yang Q, Hao J. 2023. Phylogenomics reveal extensive phylogenetic discordance due to incomplete lineage sorting following the rapid radiation of alpine butterflies (Papilionidae: Parnassius). *Syst Entomol*. 48:585-599.
Hibbins MS, Breithaupt LC, Hahn MW. 2023. Phylogenomic comparative methods: Accurate evolutionary inferences in the presence of gene tree discordance. *Proc Natl Acad Sci U S A*. 120:e2220389120.
Hinrichs AS, Karolchik D, Baertsch R, Barber GP, Bejerano G, Clawson H, Diekhans M, Furey TS, Harte RA, Hsu F, et al. 2006. The UCSC genome browser database: Update 2006. *Nucleic Acids Res*. 34:D590-598.

Hoang DT, Chernomor O, von Haeseler A, Minh BQ, Vinh LS. 2018. Ufboot2: Improving the ultrafast bootstrap approximation. *Mol Biol Evol*. 35:518-522.
Hobolth A, Christensen OF, Mailund T, Schierup MH. 2007. Genomic relationships and speciation times of human, chimpanzee, and gorilla inferred from a coalescent hidden Markov model. *PLoS Genet*. 3:e7.
Holm S. 1979. A simple sequentially rejective multiple test procedure. *Scandinavian journal of statistics*. 6:65-70.
Hu Z, Sackton TB, Edwards SV, Liu JS. 2019. Bayesian detection of convergent rate changes of conserved noncoding elements on phylogenetic trees. *Mol Biol Evol*. 36:1086-1100.
Hudson RR. 1983. Testing the constant-rate neutral allele model with protein sequence data. *Evolution*. 37:203-217.
Hudson RR, Kaplan NL. 1988. The coalescent process in models with selection and recombination. *Genetics*. 120:831-840.
Hudson RR, Kaplan NL. 1995. Deleterious background selection with recombination. *Genetics*. 141:1605-1617.
Huson DH, Klöpper T, Lockhart PJ, Steel MA. 2005. Reconstruction of reticulate networks from gene trees. In: Miyano S, Mesirov J, Kasif S, Istrail S, Pevzner PA, Waterman M, editors. Research in computational molecular biology. RECOMB 2005. Lecture Notes in Computer Science: Springer, Berlin, Heidelberg.
Jackman SD, Vandervalk BP, Mohamadi H, Chu J, Yeo S, Hammond SA, Jahesh G, Khan H, Coombe L, Warren RL, Birol I. 2017. ABySS 2.0: Resource-efficient assembly of large genomes using a Bloom filter. *Genome Res*. 27:768-777.
Jarvis ED, Mirarab S, Aberer AJ, Li B, Houde P, Li C, Ho SY, Faircloth BC, Nabholz B, Howard JT, et al. 2014. Whole-genome analyses resolve early branches in the tree of life of modern birds. *Science*. 346:1320-1331.
Jones MR, Mills LS, Alves PC, Callahan CM, Alves JM, Lafferty DJR, Jiggins FM, Jensen JD, Melo-Ferreira J, Good JM. 2018. Adaptive introgression underlies polymorphic seasonal camouflage in snowshoe hares. *Science*. 360:1355-1358.
Junier T, Zdobnov EM. 2010. The Newick utilities: High-throughput phylogenetic tree processing in the unix shell. *Bioinformatics*. 26:1669-1670.
Kalyaanamoorthy S, Minh BQ, Wong TKF, von Haeseler A, Jermiin LS. 2017. Modelfinder: Fast model selection for accurate phylogenetic estimates. *Nat Methods*. 14:587-589.
Kaplan NL, Hudson RR, Langley CH. 1989. The "hitchhiking effect" revisited. *Genetics*. 123:887-899.
Kartje ME, Jing P, Payseur BA. 2020. Weak correlation between nucleotide variation and recombination rate across the house mouse genome. *Genome Biol Evol*. 12:293-299.
Katoh K, Standley DM. 2013. Mafft multiple sequence alignment software version 7: Improvements in performance and usability. *Mol Biol Evol*. 30:772-780.
Katzman S, Kern AD, Bejerano G, Fewell G, Fulton L, Wilson RK, Salama SR, Haussler D. 2007. Human genome ultraconserved elements are ultraselected. *Science*. 317:915.
Keane TM, Wong K, Adams DJ, Flint J, Reymond A, Yalcin B. 2014. Identification of structural variation in mouse genomes. *Front Genet*. 5:192.
Kowalczyk A, Meyer WK, Partha R, Mao W, Clark NL, Chikina M. 2019. Rerconverge: An r package for associating evolutionary rates with convergent traits. *Bioinformatics*. 35:4815-4817.
Kulathinal RJ, Stevison LS, Noor MA. 2009. The genomics of speciation in Drosophila: Diversity, divergence, and introgression estimated using low-coverage genome sequencing. *PLoS Genet*. 5:e1000550.
Kumon T, Ma J, Akins RB, Stefanik D, Nordgren CE, Kim J, Levine MT, Lampson MA. 2021. Parallel pathways for recruiting effector proteins determine centromere drive and suppression. *Cell*. 184:4904-4918 e4911.

Calculating and interpreting gene- and site-concordance factors in phylogenomics [Internet]. The Lanfear Lab @ ANU2018 September 20, 2021]. Available from: http://www.robertlanfear.com/blog/files/concordance_factors.html

Lecompte E, Aplin K, Denys C, Catzeflis F, Chades M, Chevret P. 2008. Phylogeny and biogeography of African Murinae based on mitochondrial and nuclear gene sequences, with a new tribal classification of the subfamily. *BMC Evol Biol*. 8:199.

Lewontin RC, Birch LC. 1966. Hybridization as a source of variation for adaptation to new environments. *Evolution*. 20:315-336.

Li H. 2013. Aligning sequence reads, clone sequences and assembly contigs with bwa-mem. *arXiv preprint arXiv:1303.3997*.

Li H. 2018. Minimap2: Pairwise alignment for nucleotide sequences. *Bioinformatics*. 34:3094-3100.

Liu X, Wei F, Li M, Jiang X, Feng Z, Hu J. 2004. Molecular phylogeny and taxonomy of wood mice (genus Apodemus Kaup, 1829) based on complete mtDNA cytochrome b sequences, with emphasis on chinese species. *Mol Phylogenet Evol*. 33:1-15.

Lopes F, Oliveira LR, Kessler A, Beux Y, Crespo E, Cardenas-Alayza S, Majluf P, Sepulveda M, Brownell RL, Franco-Trecu V, et al. 2021. Phylogenomic discordance in the eared seals is best explained by incomplete lineage sorting following explosive radiation in the southern hemisphere. *Syst Biol*. 70:786-802.

Lundrigan BL, Jansa SA, Tucker PK. 2002. Phylogenetic relationships in the genus Mus, based on paternally, maternally, and biparentally inherited characters. *Syst Biol*. 51:410-431.

Maddison WP. 1997. Gene trees in species trees. *Systematic Biology*. 46:523-536.

Martin Y, Gerlach G, Schlotterer C, Meyer A. 2000. Molecular phylogeny of European muroid rodents based on complete cytochrome b sequences. *Mol Phylogenet Evol*. 16:37-47.

McKenzie PF, Eaton DAR. 2020. The multispecies coalescent in space and time. *bioRxiv*.2020.2008.2002.233395.

Mendes FK, Fuentes-Gonzalez JA, Schraiber JG, Hahn MW. 2018. A multispecies coalescent model for quantitative traits. *eLife*. 7:e36482.

Mendes FK, Hahn MW. 2016. Gene tree discordance causes apparent substitution rate variation. *Syst Biol*. 65:711-721.

Mendes FK, Hahn Y, Hahn MW. 2016. Gene tree discordance can generate patterns of diminishing convergence over time. *Mol Biol Evol*. 33:3299-3307.

Mendes FK, Livera AP, Hahn MW. 2019. The perils of intralocus recombination for inferences of molecular convergence. *Philos Trans R Soc Lond B Biol Sci*. 374:20180244.

Minh BQ, Hahn MW, Lanfear R. 2020a. New methods to calculate concordance factors for phylogenomic datasets. *Mol Biol Evol*. 37:2727-2733.

Minh BQ, Schmidt HA, Chernomor O, Schrempf D, Woodhams MD, von Haeseler A, Lanfear R. 2020b. Iq-tree 2: New models and efficient methods for phylogenetic inference in the genomic era. *Mol Biol Evol*. 37:1530-1534.

Mölder F, Jablonski KP, Letcher B, Hall MB, Tomkins-Tinch CH, Sochat V, Forster J, Lee S, Twardziok SO, Kanitz A, et al. 2021. Sustainable data analysis with snakemake. *F1000Res*. 10:33.

Moore EC, Thomas GWC, Mortimer S, Kopania EEK, Hunnicutt KE, Clare-Salzler ZJ, Larson EL, Good JM. 2022. The evolution of widespread recombination suppression on the dwarf hamster (Phodopus) X chromosome. *Genome Biol Evol*. 14:evac080.

Morgan AP, Gatti DM, Najarian ML, Keane TM, Galante RJ, Pack AI, Mott R, Churchill GA, de Villena FP. 2017. Structural variation shapes the landscape of recombination in mouse. *Genetics*. 206:603-619.

948 Mouse Genome Sequencing C, Waterston RH, Lindblad-Toh K, Birney E, Rogers J, Abril JF, Agarwal P,
949 Agarwala R, Ainscough R, Alexandersson M, et al. 2002. Initial sequencing and comparative
950 analysis of the mouse genome. *Nature*. 420:520-562.
951 Murrell B, Weaver S, Smith MD, Wertheim JO, Murrell S, Aylward A, Eren K, Pollner T, Martin DP, Smith
952 DM, et al. 2015. Gene-wide identification of episodic selection. *Mol Biol Evol*. 32:1365-1371.
953 Nilsson P, Solbakken MH, Schmid BV, Orr RJS, Lv R, Cui Y, Song Y, Zhang Y, Baalsrud HT, Torresen OK, et al.
954 2020. The genome of the great gerbil reveals species-specific duplication of an MHCII gene.
955 *Genome Biol Evol*. 12:3832-3849.
956 Pagès M, Fabre P-H, Chaval Y, Mortelliti A, Nicolas V, Wells K, Michaux JR, Lazzari V. 2016. Molecular
957 phylogeny of South-east Asian arboreal murine rodents. *Zoologica Scripta*. 45:349-364.
958 Pamilo P, Nei M. 1988. Relationships between gene trees and species trees. *Mol Biol Evol*. 5:568-583.
959 Paradis E, Schliep K. 2019. Ape 5.0: An environment for modern phylogenetics and evolutionary analyses
960 in r. *Bioinformatics*. 35:526-528.
961 Partha R, Kowalczyk A, Clark NL, Chikina M. 2019. Robust method for detecting convergent shifts in
962 evolutionary rates. *Mol Biol Evol*. 36:1817-1830.
963 Pease JB, Haak DC, Hahn MW, Moyle LC. 2016. Phylogenomics reveals three sources of adaptive variation
964 during a rapid radiation. *PLoS Biol*. 14:e1002379.
965 Pease JB, Hahn MW. 2013. More accurate phylogenies inferred from low-recombination regions in the
966 presence of incomplete lineage sorting. *Evolution*. 67:2376-2384.
967 Platt RN, 2nd, Vandewege MW, Ray DA. 2018. Mammalian transposable elements and their impacts on
968 genome evolution. *Chromosome Res*. 26:25-43.
969 Pollard KS, Hubisz MJ, Rosenbloom KR, Siepel A. 2010. Detection of nonneutral substitution rates on
970 mammalian phylogenies. *Genome Res*. 20:110-121.
971 Pond SL, Frost SD, Muse SV. 2005. Hyphy: Hypothesis testing using phylogenies. *Bioinformatics*. 21:676-
972 679.
973 Poplin R, Ruano-Rubio V, DePristo MA, Fennell TJ, Carneiro MO, Auwera GAV, Kling DE, Gauthier LD, Levy-
974 Moonshine A, Roazen D, et al. 2018. Scaling accurate genetic variant discovery to tens of
975 thousands of samples. *bioRxiv*.201178.
976 Quinlan AR, Hall IM. 2010. Bedtools: A flexible suite of utilities for comparing genomic features.
977 *Bioinformatics*. 26:841-842.
978 R Core Team. 2021. R: A language and environment for statistical computing. Vienna, Austria.
979 Ranwez V, Douzery EJP, Cambon C, Chantret N, Delsuc F. 2018. Macse v2: Toolkit for the alignment of
980 coding sequences accounting for frameshifts and stop codons. *Mol Biol Evol*. 35:2582-2584.
981 Revell LJ. 2012. Phytools: An r package for phylogenetic comparative biology (and other things). *Methods
982 in Ecology and Evolution*. 3:217-223.
983 Rivas-Gonzalez I, Rousselle M, Li F, Zhou L, Dutheil JY, Munch K, Shao Y, Wu D, Schierup MH, Zhang G.
984 2023. Pervasive incomplete lineage sorting illuminates speciation and selection in primates.
985 *Science*. 380:eabn4409.
986 Robinson DF, Foulds LR. 1981. Comparison of phylogenetic trees. *Mathematical Biosciences*. 53:131-147.
987 Robinson DF, Foulds LR editors.; 1979. Proc 6th Australian Conf Combinatorial Mathematics, Lecture
988 Notes in Mathematics. Berlin, Heidelberg.
989 Romanenko SA, Perelman PL, Trifonov VA, Graphodatsky AS. 2012. Chromosomal evolution in Rodentia.
990 *Heredity (Edinb)*. 108:4-16.
991 Rosenberg NA. 2002. The probability of topological concordance of gene trees and species trees. *Theor
992 Popul Biol*. 61:225-247.
993 Rowe KC, Achmadi AS, Fabre P-H, Schenk JJ, Steppan SJ, Esselstyn JA. 2019. Oceanic islands of Wallacea
994 as a source for dispersal and diversification of murine rodents. *Journal of Biogeography*. 46:2752-
995 2768.

996 Roycroft E, Achmadi A, Callahan CM, Esselstyn JA, Good JM, Moussalli A, Rowe KC. 2021. Molecular
997 evolution of ecological specialisation: Genomic insights from the diversification of murine
998 rodents. *Genome Biol Evol*. 13:evab103.
999 Roycroft EJ, Moussalli A, Rowe KC. 2020. Phylogenomics uncovers confidence and conflict in the rapid
1000 radiation of Australo-Papuan rodents. *Syst Biol*. 69:431-444.
1001 Sarver BA, Keeble S, Cosart T, Tucker PK, Dean MD, Good JM. 2017. Phylogenomic insights into mouse
1002 evolution using a pseudoreference approach. *Genome Biol Evol*. 9:726-739.
1003 Scally A, Dutheil JY, Hillier LW, Jordan GE, Goodhead I, Herrero J, Hobolth A, Lappalainen T, Mailund T,
1004 Marques-Bonet T, et al. 2012. Insights into hominid evolution from the gorilla genome sequence.
1005 *Nature*. 483:169-175.
1006 Schenk JJ, Rowe KC, Steppan SJ. 2013. Ecological opportunity and incumbency in the diversification of
1007 repeated continental colonizations by muroid rodents. *Syst Biol*. 62:837-864.
1008 Schliep KP. 2011. Phangorn: Phylogenetic analysis in r. *Bioinformatics*. 27:592-593.
1009 Serizawa K, Suzuki H, Tsuchiya K. 2000. A phylogenetic view on species radiation in Apodemus inferred
1010 from variation of nuclear and mitochondrial genes. *Biochem Genet*. 38:27-40.
1011 Shifman S, Bell JT, Copley RR, Taylor MS, Williams RW, Mott R, Flint J. 2006. A high-resolution single
1012 nucleotide polymorphism genetic map of the mouse genome. *PLoS Biol*. 4:e395.
1013 Slatkin M, Pollack JL. 2006. The concordance of gene trees and species trees at two linked loci. *Genetics*.
1014 172:1979-1984.
1015 Smagulova F, Gregoretti IV, Brick K, Khil P, Camerini-Otero RD, Petukhova GV. 2011. Genome-wide analysis
1016 reveals novel molecular features of mouse recombination hotspots. *Nature*. 472:375-378.
1017 Repeatmasker open-4.0 [Internet]. 2013-2015. Available from http://www.repeatmasker.org.
1018 Smith BT, Merwin J, Provost KL, Thom G, Brumfield RT, Ferreira M, Mauck WM, Moyle RG, Wright TF,
1019 Joseph L. 2023. Phylogenomic analysis of the parrots of the world distinguishes artifactual from
1020 biological sources of gene tree discordance. *Syst Biol*. 72:228-241.
1021 Smith JM, Haigh J. 1974. The hitch-hiking effect of a favourable gene. *Genet Res*. 23:23-35.
1022 Smith MD, Wertheim JO, Weaver S, Murrell B, Scheffler K, Kosakovsky Pond SL. 2015a. Less is more: An
1023 adaptive branch-site random effects model for efficient detection of episodic diversifying
1024 selection. *Mol Biol Evol*. 32:1342-1353.
1025 Smith SA, Brown JW, Walker JF. 2018. So many genes, so little time: A practical approach to divergence-
1026 time estimation in the genomic era. *PLoS One*. 13:e0197433.
1027 Smith SA, Moore MJ, Brown JW, Yang Y. 2015b. Analysis of phylogenomic datasets reveals conflict,
1028 concordance, and gene duplications with examples from animals and plants. *BMC Evol Biol*.
1029 15:150.
1030 Stanyon R, Yang F, Cavagna P, O'Brien P, Bagga M, Ferguson-Smith M, Wienberg J. 1999. Animal
1031 cytogenetics and comparative mapping-reciprocal chromosome painting shows that genomic
1032 rearrangement between rat and mouse proceeds ten times faster than between humans and cats.
1033 *Cytogenetics and Cell Genetics*. 84:150-155.
1034 Steppan SJ, Adkins RM, Spinks PQ, Hale C. 2005. Multigene phylogeny of the Old World mice, Murinae,
1035 reveals distinct geographic lineages and the declining utility of mitochondrial genes compared to
1036 nuclear genes. *Mol Phylogenet Evol*. 37:370-388.
1037 Steppan SJ, Schenk JJ. 2017. Muroid rodent phylogenetics: 900-species tree reveals increasing
1038 diversification rates. *PLoS One*. 12:e0183070.
1039 Sun C, Huang J, Wang Y, Zhao X, Su L, Thomas GWC, Zhao M, Zhang X, Jungreis I, Kellis M, et al. 2021.
1040 Genus-wide characterization of bumblebee genomes provides insights into their evolution and
1041 variation in ecological and behavioral traits. *Mol Biol Evol*. 38:486-501.

Suzuki H, Shimada T, Terashima M, Tsuchiya K, Aplin K. 2004. Temporal, spatial, and ecological modes of evolution of Eurasian Mus based on mitochondrial and nuclear gene sequences. *Mol Phylogenet Evol*. 33:626-646.
Tange O. 2018. Gnu parallel.
To TH, Jung M, Lycett S, Gascuel O. 2016. Fast dating using least-squares criteria and algorithms. *Syst Biol*. 65:82-97.
Treaster S, Deelen J, Daane JM, Murabito J, Karasik D, Harris MP. 2023. Convergent genomics of longevity in rockfishes highlights the genetics of human life span variation. *Sci Adv*. 9:eadd2743.
van der Valk T, Pecnerova P, Diez-Del-Molino D, Bergstrom A, Oppenheimer J, Hartmann S, Xenikoudakis G, Thomas JA, Dehasque M, Saglican E, et al. 2021. Million-year-old DNA sheds light on the genomic history of mammoths. *Nature*. 591:265-269.
Vanderpool D, Minh BQ, Lanfear R, Hughes D, Murali S, Harris RA, Raveendran M, Muzny DM, Hibbins MS, Williamson RJ, et al. 2020. Primate phylogenomics uncovers multiple rapid radiations and ancient interspecific introgression. *PLoS Biol*. 18:e3000954.
Wang LG, Lam TT, Xu S, Dai Z, Zhou L, Feng T, Guo P, Dunn CW, Jones BR, Bradley T, et al. 2020. Treeio: An r package for phylogenetic tree input and output with richly annotated and associated data. *Mol Biol Evol*. 37:599-603.
White MA, Ane C, Dewey CN, Larget BR, Payseur BA. 2009. Fine-scale phylogenetic discordance across the house mouse genome. *PLoS Genet*. 5:e1000729.
Yalcin B, Wong K, Agam A, Goodson M, Keane TM, Gan X, Nellaker C, Goodstadt L, Nicod J, Bhomra A, et al. 2011. Sequence-based characterization of structural variation in the mouse genome. *Nature*. 477:326-329.
Yang Z. 2007. Paml 4: Phylogenetic analysis by maximum likelihood. *Mol Biol Evol*. 24:1586-1591.
Yekutieli D, Benjamini Y. 1999. Resampling-based false discovery rate controlling multiple test procedures for correlated test statistics. *Journal of Statistical Planning and Inference*. 82:171-196.
Yu G. 2020. Using ggtree to visualize data on tree-like structures. *Curr Protoc Bioinformatics*. 69:e96.
Yu G, Smith DK, Zhu H, Guan Y, Lam TT-Y. 2017. Ggtree: An r package for visualization and annotation of phylogenetic trees with their covariates and other associated data. *Methods in Ecology and Evolution*. 8:28-36.
Zhang C, Rabiee M, Sayyari E, Mirarab S. 2018. Astral-iii: Polynomial time species tree reconstruction from partially resolved gene trees. *BMC Bioinformatics*. 19:153.